ACS APPLIED MATERIALS & INTERFACES

Research Article

www.acsami.org

One-Step Synthesis of Nanoscale Zeolitic Imidazolate Frameworks with High Curcumin Loading for Treatment of Cervical Cancer

Min Zheng,[†,‡,§] Shi Liu,[†] Xingang Guan,[†] and Zhigang Xie*[,†]

[†]State Key Laboratory of Polymer Physics and Chemistry, Changchun Institute of Applied Chemistry, Chinese Academy of Sciences, 5625 Renmin Street, Changchun, Jilin 130022, P. R. China

[‡]Chemistry and Life Science School, Advanced Institute of Materials Science, Changchun University of Technology, 2055 Yanan Street, Changchun, Jilin 130012, P. R. China

[§]State Key Laboratory of Luminescence and Applications, Changchun Institute of Optics, Fine Mechanics, and Physics, Chinese Academy of Sciences, 3888 East Nanhu Road, Changchun, Jilin 130033, P. R. China

Supporting Information

ABSTRACT: A straightforward nanoprecipitating method was developed to prepare water dispersible curcumin (CCM)-loaded nanoscale zeolitic imidazolate framework-8 (CCM@NZIF-8) nanoparticles (NPs). The as-synthesized CCM@NZIF-8 NPs possess high drug encapsulation efficiency (88.2%), good chemical stability and fast drug release in tumor acidic microenvironments. Confocal laser scanning microscopy and cytotoxicity experiments reveal that NZIF-8 based nanocarriers promote the cellular uptake of CCM and result in higher cytotoxicity of CCM@NZIF-8 than that of free CCM toward HeLa cells. The in vivo anticancer experiments indicate that CCM@NZIF-8 NPs exhibit much higher antitumor efficacy than free CCM. This work highlights the potential of using nanoscale metal organic framworks (NMOFs) as a simple and stable platform for developing a highly efficient drug delivery system in cancer treatment.

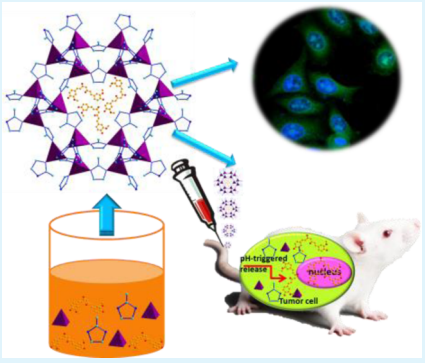

KEYWORDS: *ZIF-8, curcumin, nanocarrier, drug delivery, cervical cancer*

INTRODUCTION

Curcumin (CCM), a natural chemotherapeutic agent with highly biocompatible and biodegradable properties, has attracted considerable attention for its significantly wide spectrum of therapeutic effects on human health such as antitumor, antioxidant, and antibacterial activities.[1−8] However, free CCM cannot be administered systemically due to its high hydrophobicity and poor bioavailability. Although various attempts have been made to encapsulate CCM in inorganic-based carriers such as silica[9] NPs or organic-based carriers exampling cyclodextrin,[10] micelles,[11−14] and liposomes[15,16] NPs, etc. to render CCM dispersible in aqueous media, the synthesis process of these NPs was relatively complicated and time-consuming. Therefore, it is highly desired to develop a simple and efficient methodology for the incorporation CCM into nanocarriers.

Metal−organic frameworks (MOFs) are an emerging class of hybrid crystalline porous materials that are constructed from organic bridging ligands and metal ion connectors.[17−23] Known for their large porosity with high surface area, tunable shapes and pore sizes, and controllable surface functionalities, MOFs have been utilized in a wide range of applications such as heterogeneous catalysis,[24−33] gas storage[34−42] and chemical sensing[43−51] etc. When scaled down into the nanoregime, nanoscale MOFs (NMOFs) promise to be a powerful platform for the delivery and controlled release of drug molecules by virtue of their nanoscale sizes and high porosity.[52−60] In the past several years, some pioneering studies have demonstrated the great potential of NMOFs as drug carriers. However, challenges still remain in the design of functional NMOFs that meet the stringent requirements of biological systems, including biocompatibility of both the metal and bridging ligand, stability of NMOFs in biological environment, and controlled drug release in the targeted sites. Zeolitic imidazolate framework-8 (NZIF-8),[61−63] constructed from zinc ions and 2-methyl imidazole (MIM), showing excellent biocompatibility and pH-sensitive behavior, which is an ideal nanocarrier for drug delivery. Although a few groups undertook some attempts to incorporate some drugs into nanoscale ZIF-8 (NZIF-8),[64,65] the lower drug loading and poor stability in biological environment limited their progress in tumor treatment. To the best of our knowledge, no work on using NZIF-8 based drug delivery system for in vivo anticancer therapy is reported.

In the present work, natural anticancer drug CCM was encapsulated into NZIF-8 via a simple, rapid, and universal route under mild conditions (Scheme 1). The obtained CCM@NZIF-8 NPs have uniform sizes and morphologies with an average diameter of 119.3 ± 13.6 nm. The drug loading

Received: May 18, 2015
Accepted: September 25, 2015
Published: September 25, 2015

DOI: 10.1021/acsami.5b04315
ACS Appl. Mater. Interfaces 2015, 7, 22181−22187

Scheme 1. Schematic Illustration of the Preparation of CCM@NZIF-8 and Its Application for in Vitro Bioimaging and in Vivo Anticancer Therapy

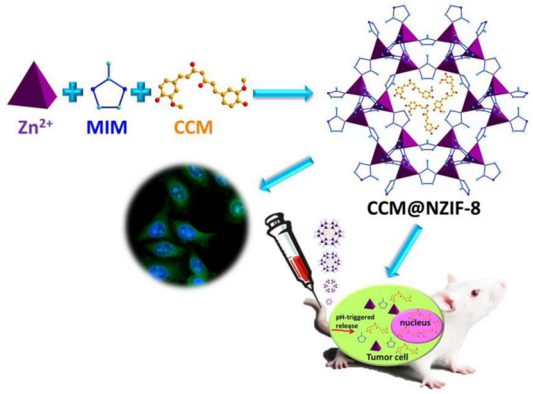

capability (DLC) and drug loading encapsulation efficiency (DLE) of CCM@NZIF-8 was determined to be 12.7% and 88.2%, respectively. The high stability of CCM@NZIF-8 in phosphate-buffered saline (PBS) pH 7.4 or fetal calf serum solutions (FBS) was confirmed by dynamic light scattering (DLS). The cytotoxicity toward HeLa cells revealed that CCM@NZIF-8 exhibited higher inhibition efficiency than free CCM. The in vivo antitumor effect experiments in xenograft tumor model (U14 cervical cancer) displayed that CCM@NZIF-8 could inhibit cervical cancer cell growth with tumor inhibitory rate of 85%, while the tumor inhibitory rate of free CCM was 43%, confirming that CCM@NZIF-8 has much higher bioavailability than that of free CCM. All of the experiment results reveal that CCM@NZIF-8 systems are promising for cancer therapy and are beneficial for targeting cancerous tissues.

RESULTS AND DISCUSSION

In order to realize the efficient encapsulation of CCM into the framework of NZIF-8, the reaction conditions were screened and optimized in terms of solvents, reaction time, and the weight ratio of CCM to MIM and $Zn(NO_3)_2$. First, we repeated the previous method[66] reported by Zhuang et al. with some modification (see the Supporting Information, Table S1); however, the DLC and DLE was determined to be as low as 0.33% and 2.05% (entry 1), respectively, according to the characteristic absorption peak of CCM at 427 nm (see Supporting Information, Figure S1). Although increasing the weight ratio of CCM to MIM and $Zn(NO_3)_2$ can enhance slightly the DLC and DLE (Table S2), the morphologies and sizes of the samples changed from ~200 nm NPs (entry 1, Figure S2) to microflowers with diameters ~3 μm (entry 3, Figure S3), which might be attributed to intermolecular hydrogen bond between the nitrogen atom in MIM and the phenolic hydroxyl group in CCM, such big particles are not suitable as drug carriers. Then, a simple nanoprecipitating method was developed to synthesize CCM@NZIF-8 NPs by mixing the aqueous of $Zn(NO_3)_2$ with the MeOH or THF solution of MIM and CCM (see the Supporting Information) in 1 min. When THF was used as solvent to dissolve MIM and CCM (entry 4), the obtained NPs are as small as ~50 nm (Figure S4), and the DLC and DLE was only 1.16% and 6.72%, respectively. When MeOH was used as solvent, DLC and DLE was enhanced dramatically (entries 5 and 6), and the optimized condition was concluded to be 5 mL of $Zn(NO_3)_2$ (150 mg) aqueous solution was added into the MeOH (10 mL) solution of MIM (330 mg) and CCM (5 mg, 1 wt %) under vigorous stirring, and only 1 min later, CCM@NZIF-8 NPs were formed. The obtained NPs was collected by centrifugation and then washed with methanol three times. As a control experiment, NZIF-8 NPs were synthesized via the similar route. The drawback of poor water solubility of CCM was circumvented by loading CCM into NZIF-8 NPs, the DLC and

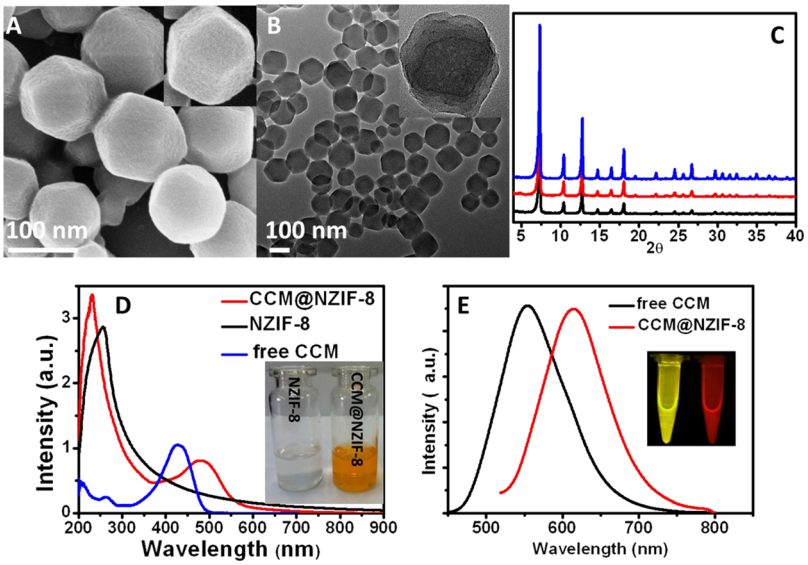

Figure 1. (A) SEM image of CCM@NZIF-8 NPs, (B) TEM image of CCM@NZIF-8 NPs, zoom-in on a single NPs. (C) XRD patterns of simulated ZIF-8 (black solid line), NZIF-8 (red solid line), and CCM@NZIF-8 (blue solid line). (D) The UV−vis absorption of NZIF-8 (black solid line), free CCM (blue solid line), and CCM@NZIF-8 (red solid line) in methanol solution, inset is the photos of NZIF-8 and CCM@NZIF-8. (E) The PL spectra of free CCM (black solid line) and CCM@NZIF-8 (red solid line), inset are the photos of free CCM and CCM@NZIF-8 under the excitation of blue light (445−490 nm).

DOI: 10.1021/acsami.5b04315
ACS Appl. Mater. Interfaces 2015, 7, 22181−22187

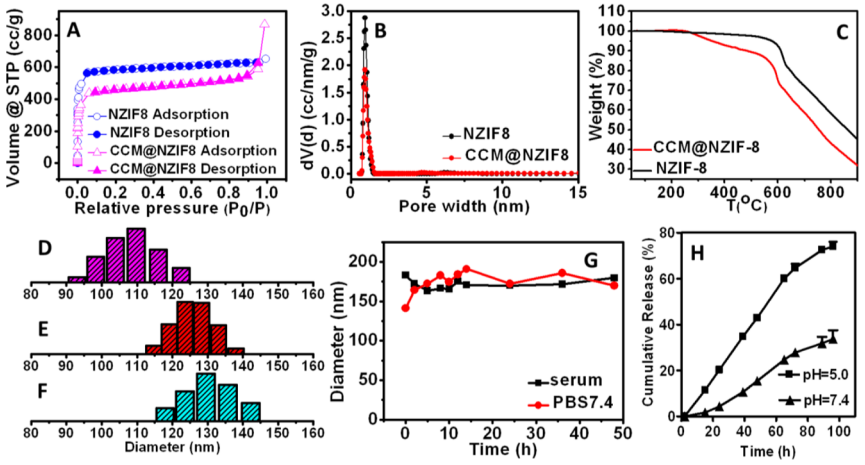

Figure 2. (A) Nitrogen-sorption isotherms, (B) pore-size distributions, and (C) TGA curves of the as-synthesized NZIF-8 and CCM@ZIF-8 NPs. Particle size distributions of (D) NZIF-8, (E) CCM@NZIF-8, and (F) CCM@NZIF-8 after kept for 1 month determined by DLS. (G) Hydrodynamic diameters of CCM@NZIF-8 NPs in PBS (pH 7.4) and fetal calf serum. (H) CCM release profiles from CCM@NZIF-8 in PBS solution (pH 5.0 and 7.4) containing 1 wt % of Tween-80.

DLE of CCM@NZIF-8 was determined to be 12.7% and 88.2%, respectively, such high DLC is crucial to the effective treatment of solid tumors. Scanning electron microscopy (SEM) and transmission electron microscopy (TEM) were used to characterize the morphologies and sizes of CCM@NZIF-8 and NZIF-8, Figure 1A,B reveals that CCM@NZIF-8 NPs are uniform rhombic dodecahedral particles with narrow size distribution, which are similar to those of NZIF-8 (Figures S5 and S6). As determined from the SEM image, these particles have an average diameter of 119.3 ± 13.6 nm. Figure 1C shows the powder XRD patterns (PXRD) of the as-synthesized CCM@NZIF-8 (blue line), NZIF-8 (red line), and simulated ZIF-8 (black line), and the results indicate that CCM@NZIF-8 has pure-phase ZIF-8.[67] The UV−vis absorption spectra of NZIF-8, free CCM, and CCM@NZIF-8 are shown in Figure 1D; no characteristic absorption band is observed for NZIF-8, while after incorporation of CCM into NZIF-8, CCM@NZIF-8 has a strong absorption band centered at 485 nm which is red-shifted 57 nm relative to that of free CCM, indicating that CCM was encapsulated into the framework of NZIF-8. The photoluminescence (PL) spectra (Figure 1E) of free CCM and CCM@NZIF-8 show that the PL peak of CCM@NZIF-8 is centered at 615 nm, which is bathochromic-shifted by 61 nm relative to that of free CCM, further approving the incorporation of CCM into NZIF-8. The zeta potential value of CCM@NZIF-8 is about +4.3 mV, which is similar to that of NZIF-8 (+ 4.4 mV) confirming that CCM was not adsorbed onto the surface of NZIF-8 but loaded into its framework.

The porosities of NZIF-8 and CCM@NZIF-8 NPs were investigated by nitrogen-sorption measurements. As shown in Figure 2A, the as-prepared CCM@NZIF-8 NPs exhibit a type I isotherm, with significant increases in N_2 uptake at very low relative pressure (<0.01) due to the presence of micropores, as does NZIF-8. The gravimetric Brunauer−Emmett−Teller (BET) surface area of CCM@NZIF-8 is 1826 m^2/g, which is lower than that of NZIF-8 (2370 m^2/g), the slight decrease of the porosity of CCM@NZIF-8 is ascribed to the encapsulating of CCM into the NZIF-8 framework. The pore-size distribution of the MOF matrix (Figure 2B) is not altered after the incorporation of CCM. The thermogravimetric analysis (TGA) of NZIF-8 and CCM@NZIF-8 was performed under nitrogen flow. As shown in Figure 2C, a long plateau was observed in the temperature range of 50−588 °C (NZIF-8), indicating the high thermal stability of NZIF-8. While the TGA curve of CCM@NZIF-8 exhibit a gradual weight loss of 13.4% up to 547 °C, corresponding to the removal of CCM from the cavities, implying that about 13.4 wt % of CCM was loaded into the framework, which is consistent with the results determined by UV−vis standard curves. DLS was used to study the size distribution of NPs. As shown in Figure 2E, the hydrodynamic diameters of the CCM@NZIF-8 NPs possess a narrow size distribution with the peak value of 124 nm, which is a little larger than that of NZIF-8 (110 nm, Figure 2D). The nanoscale sizes (<200 nm) were beneficial to increase passive tumor targeting due to the enhanced permeation and retention effect (EPR).[68,69]

The stability of NPs is very important for their cell internalization and circulation in blood. First, we studied the stability of CCM@NZIF-8 NPs in MeOH solution, the NPs was kept for 1 month, and no precipitate was formed. The hydrodynamic diameter (Figure 2F) determined by DLS indicated that no obvious size change was observed, implying the high stability of CCM@NZIF-8. Second, the hydrodynamic diameters were monitored in phosphate-buffered saline (PBS) pH 7.4 or fetal calf serum solutions (FBS) with the concentration of 0.1 mg/mL. As shown in Figure S7 and Figure 2G, the hydrodynamic diameters of NZIF-8 and CCM@NZIF-8 NPs in both PBS and FBS did not change significantly, indicating that no aggregation or dissociation occurred during 48 h of incubation. The stability of CCM in different solutions was studied by UV−vis absorption spectroscopy (Figure S8). CCM degraded rapidly in 0.02 M phosphate buffered saline (PBS, pH 7.4), about 92% of CCM decomposed in 4 min (Figure S8A), while 44% of CCM remained after 4 h of incubation in PBS (pH 5.0), indicating it is more stable in acidic condition (Figure S8B). The stability of CCM was strongly improved by adding 1 wt % of Tween-80 into the PBS solutions. As shown in Figure S8C,D, only 4% or 9% of CCM decomposed in PBS (pH 5.0)/Tween-80 (1 wt %) or PBS (pH 7.4)/Tween-80 (1 wt %), respectively, even after 48 h of incubation. Hence, Tween-80 acts as not only a solubilizer but also a stabilizer. In vitro drug release experiments were performed in PBS (pH 7.4 and 5.0)/Tween-80 (1 wt %) to evaluate its controlled release behavior. As shown in Figure 2H,

DOI: 10.1021/acsami.5b04315
ACS Appl. Mater. Interfaces 2015, 7, 22181−22187

in acidic PBS solution (pH 5.0), the cumulative release of CCM reached to 43.4% after 48 h. In contrast, the CCM@NZIF-8 NPs show very slow drug release rates, only 15.6% of CCM was released even after 48 h in neutral PBS (pH 7.4). The pH-responsive release feature of NZIF-8 can diminish premature drug release during blood circulation but specifically enhance drug release due to the acidic microenvironments of tumors sites, which will be definitely beneficial for tumor inhibition in vivo.

Before NZIF-8 was used for drug carrier, cellular biocompatibility experiments were carried out by standard 3-(4,5-dimethyl-thiazol-2-yl)-2,5-diphenyltetrazolium bromide (MTT) assay with human epithelial carcinoma cells (HeLa cell line) as the test cell line. As shown in Figure 3A, when

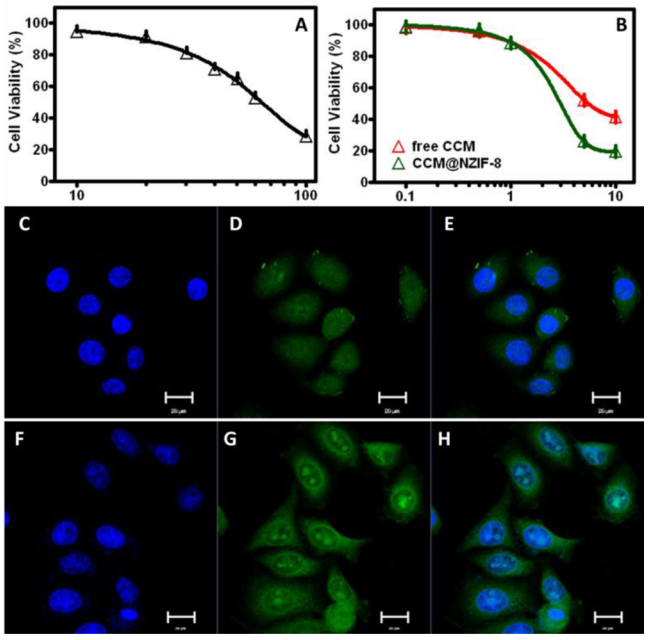

Figure 3. (A) In vitro biocompatibility of NZIF-8 and (B) in vitro cytotoxicity of free CCM and CCM@NZIF-8 against HeLa cells at different concentrations for 48 h. Confocal laser-scanning microscopy (CLSM) images on HeLa cells incubated with free CCM (C–E) and CCM@NZIF-8 (F–H) at the equivalent CCM concentration (10 μg/mL) for 0.5 h, respectively. Each series can be classified to the cell nucleus (blue fluorescence, stained by DAPI), free CCM or CCM@NZIF-8 (green fluorescence, FITC channel), and the overlay image in FITC and DAPI channels on the same cell; all scale bars are 20 μm.

HeLa cells incubated with NZIF-8 at the concentrations from 10 to 50 μg/mL for 48 h, all of the survival rates exceed 70% relative to the control group cells without NZIF-8 treatment, indicating that NZIF-8 possesses negligible inhibition effects on cell proliferation below the concentration of 50 μg mL^{-1}. The half maximal effective concentration (EC_{50}) of NZIF-8 NPs was determined to be 63.8 μg/mL, which is higher than previously reported EC_{50} values (45.0 μg/mL) for NZIF-8,[66] indicating the as-obtained NZIF-8 has good biocompatibility and can be used as safe drug nanocarriers for cancer therapy. MTT experiments were also conducted to test the cytotoxicity of free CCM and CCM@NZIF-8 toward HeLa cells. As shown in Figure 3B, CCM@NZIF-8 shows higher cytotoxicity than that of free CCM with the concentrations from 1.0 to 10.0 μg/mL, the half growth inhibition concentration (IC_{50}) values of free CCM and CCM@NZIF-8 are 5.4 and 3.0 μg/mL, respectively, implying that CCM@NZIF-8 exhibits higher inhibition efficiency than free CCM on HeLa cells. The enhanced cytotoxicity can be attributed to the effective endocytosis of CCM@NZIF-8 by HeLa cells. Furthermore, confocal laser scanning microscopy (CLSM) analysis was carried out to evaluate the cellular internalization and intracellular CCM release. As shown in Figure 3, after incubation of free CCM (Figure 3C–E) and CCM@NZIF-8 (Figure 3F–H) with HeLa cells for only 0.5 h, the mean fluorescence intensity (Figure S9) of HeLa cells incubated with CCM@NZIF-8 is much stronger than that of the cells incubated with free CCM, implying that NZIF-8 based nanocarriers promote the cellular uptake of CCM. It is worthwhile noting that the fluorescence came from both the cytoplasm and nucleus region, indicating that CCM@NZIF-8 was endocytosed into the cells and CCM had been released from NZIF-8. Then the colocalized with lysosome tracker were carried out to study the way of endocytosis. Endolysosomal trafficking is a classic consequence of clathrin-mediated endocytosis from early and late endosomes to lysosomes. As shown in Figure S10, the green of CCM overlaps perfectly with the red of lysosome tracker, which confirms the clathrin-mediated endocytosis.

The xenograft tumor of U14 cervical cancer was established to evaluate the in vivo antitumor effect of CCM@NZIF-8. Because the solubility of free CCM in aqueous solution is as low as 2.99×10^{-8} M,[11] it cannot be administered systemically. In this work, free CCM was dissolved in a mixture of cremophor eL and ethanol (1:1, v/v) and this stock solution was diluted with sterile saline before injection. When the tumor grew to a size of ~200 mm^3, U14 bearing Kunming mice were randomly divided into three groups with 6 mice in each group. The free CCM or CCM@NZIF-8 groups were treated with CCM or CCM@NZIF-8 via tail-vein injection six times at 2 day intervals with the same dosage of (2.5 mg CCM)/(kg body weight), and the tumor sizes were measured every other day. The relative tumor volume V_t/V_0 as a function of time was used to investigate the inhibitory effect of CCM and CCM@NZIF-8. As shown in Figure 4A, the relative tumor volume is in an order of saline > free CCM ≫ CCM@NZIF-8 group indicating that CCM@NZIF-8 showed obvious higher antitumor efficacy than free CCM on U14 tumor cell. There is statistically a significant difference between CCM@NZIF-8 and CCM or saline. After 14 days of treatment, the sequence of relative body weight (Figure 4B) for the three groups is CCM@NZIF-8 > saline > free CCM, revealed that CCM@NZIF-8 had lower systemic toxicity than free CCM. Fourteen days later, the mice were sacrificed and the tumors were excised and weighed. The photo of the excised tumors is shown in Figure 4C, and the average weights of the tumors for saline, free CCM, and CCM@NZIF-8 groups are 5.98 ± 1.39 g, 3.38 ± 0.9 g, and 0.9 ± 0.23 g, respectively; and the tumor inhibitory rate of the CCM@NZIF-8 group is concluded to be 85%, which is much higher than that of free CCM (43%). The micrographs of H&E-stained tumor sections showed that a large area of necrosis was induced in the tumor by CCM@NZIF-8 (Figure 4F), whereas no obvious degeneration or necrosis of tumor cells occurred in the free CCM (Figure 4E) and saline group (Figure 4D) (exclusive of spontaneous necrosis in the central zone of the tumor). The results confirmed that CCM@NZIF-8 could efficiently inhibit the proliferation of U14 cervical cancer in mice. Therefore, both the in vitro and in vivo anticancer experiments indicate that CCM@NZIF-8 has much higher antitumor effect than free

DOI: 10.1021/acsami.5b04315
ACS Appl. Mater. Interfaces 2015, 7, 22181–22187

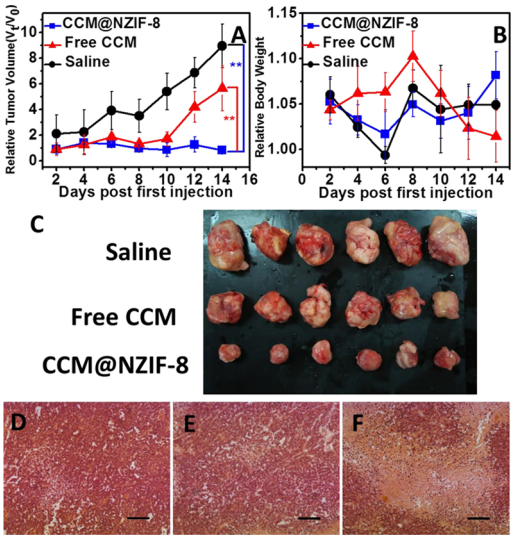

Figure 4. In vivo antitumor efficacy of CCM@NZIF-8. The relative tumor volume (A) and relative body weight (B) of the U14 cancer bearing mice as a function of time (2.5 mg CCM)/(kg body weight). (C) Photo of the excised tumors on the 14th day, $^{**}P < 0.01$. H&E staining photomicrographs of tumor tissue after treatment with (D) saline, (E) free CCM, and (F) CCM@NZIF-8 for 14 days; all the scale bars are 100 μm.

CCM and NZIF-8 might be used as the effective drug delivery system for the treatment of carcinoma.

CONCLUSION

In summary, we have developed a facile and efficient approach for the preparation of water dispersible CCM-loaded NZIF-8 (CCM@NZIF-8) NPs. The CCM@NZIF-8 NPs possess high DLE (88.2%) and DLC (12.7 wt %), excellent biocompatibility, and high stability at physiological conditions, which are ideal candidate carriers for drug delivery. The in vitro and in vivo anticancer experiments confirm that CCM@NZIF-8 NPs display much higher antitumor efficacy than free CCM, which hold immense potential in the areas of drug delivery. This work highlights the potential of using NMOF as a simple and stable platform for developing a highly efficient drug delivery system in cancer treatment.

METHODS

Synthesis of CCM-Encapsulated NZIF-8 (CCM@NZIF-8). For a typical synthesis, 150 mg of zinc nitrate hexahydrate was dissolved in 5 mL of deionized water; on the other hand, 330 mg of 2-methyl imidazole and 5 mg of CCM were dissolved into 10 mL of methanol. Under stirring, the aqueous of zinc nitrate was added into the solution of 2-methyl imidazole and CCM, the orange reaction solution became milky in 1 min, indicating that CCM@NZIF-8 nanoparticles were formed. The solution was centrifuged at 10 000 rpm for 15 min to obtain the CCM@NZIF-8. Then CCM@NZIF-8 was washed with methanol (20 mL each time) three times to completely remove the unreacted reagents. Finally, CCM@NZIF-8 particles were suspended in methanol (5 mL) for storage. In order to determine the reaction yield, 0.2 mL of dispersion was dried and weighted to calculate that 31 mg of CCM@NZIF-8 was obtained for a single synthesis. In order to measure CCM drug loading capability (DLC) and drug loading encapsulation efficiency (DLE), the dry sample was completely decomposed by 50 μL of HCl (2M) and the CCM solution was diluted to 2 mL with ethanol. The resulting clear yellow CCM solution was analyzed with a UV−vis spectrophotometer at 427 nm using a standard curve method (Figure S1). The DLC and DLE of CCM@NZIF-8 was calculated to be 12.7% and 88.2%, respectively, according to the below equation:

$$\text{DLC}\,(\%) = (\text{amount of loaded drug})/(\text{amount of drug loaded NPs}) \times 100\%$$

$$\text{DLE}\,(\%) = (\text{amount of loaded drug})/(\text{total amount of feeding drug}) \times 100\%$$

In Vitro Drug Release. In order to improve the solubility and stability of CCM, the mixed solutions of Tween-80 (1.0 wt %) with phosphate buffered saline (PBS, pH 7.4 and pH 5.0) were used as medias to study the controlled release behaviors of CCM@NZIF-8. The maximum solubility of the CCM in PBS (pH 5.0 and 7.4) solution containing Tween-80 (1.0%, w/w) is 65 μg/mL and 69 μg/mL, respectively. CCM@NZIF-8 (3 mg) was suspended in 2 mL of solutions containing Tween-80, sealed in a dialysis bag (Mw cutoff, 3.5 kDa) and incubated in the release medium (8 mL) at 37 °C under oscillation. At selected time intervals, 1 mL of buffer solution outside the dialysis bag was removed for UV−vis analysis and replaced with 1 mL of fresh buffer solution. The released amount of CCM was determined from the absorbance at 427 nm with the help of a calibration curve of CCM in the same buffer. Then the accumulative weight and relative percentage of the released CCM were calculated as a function of incubation time.

ASSOCIATED CONTENT

Supporting Information

The Supporting Information is available free of charge on the ACS Publications website at DOI: 10.1021/acsami.5b04315.

Materials, general measurements, control experiments, additional table and figures as described in the text (PDF)

AUTHOR INFORMATION

Corresponding Author

*E-mail: xiez@ciac.ac.cn.

Notes

The authors declare no competing financial interest.

ACKNOWLEDGMENTS

This project was supported by National Natural Science Foundation of China (Grants 91227118 and 21201159).

REFERENCES

(1) Srivastava, R. M.; Singh, S.; Dubey, S. V.; Misra, K.; Khar, A. Immunomodulatory and Therapeutic Activity of Curcumin. *Int. Immunopharmacol.* **2011**, *11*, 331−341.

(2) Perry, M. C.; Demeule, M.; Regina, A.; Moumdjian, R.; Beliveau, R. Curcumin Inhibits Tumor Growth and Angiogenesis in Glioblastoma Xenografts. *Mol. Nutr. Food Res.* **2010**, *54*, 1192−1201.

(3) Xu, Y.; Zhang, J.; Han, J.; Pan, X.; Cao, Y.; Guo, H.; Pan, Y.; An, Y.; Li, X. Curcumin Inhibits Tumor Proliferation Induced by Neutrophil Elastase through The Upregulation of Alpha1-Antitrypsin in Lung Cancer. *Mol. Oncol.* **2012**, *6*, 405−417.

(4) Kunwar, A.; Barik, A.; Mishra, B.; Rathinasamy, K.; Pandey, R.; Priyadarsini, K. I. Quantitative Cellular Uptake, Localization and Cytotoxicity of Curcumin in Normal and Ttumor Cells. *Biochim. Biophys. Acta, Gen. Subj.* **2008**, *1780*, 673−679.

(5) Patzko, A.; Bai, Y.; Saporta, M. A.; Katona, I.; Wu, X.; Vizzuso, D.; Feltri, M. L.; Wang, S.; Dillon, L. M.; Kamholz, J.; Kirschner, D.; Sarkar, F. H.; Wrabetz, L.; Shy, M. E. Curcumin Derivatives Promote Schwann Cell Differentiation and Improve Neuropathy in R98C CMT1B Mice. *Brain* **2012**, *135*, 3551−3566.

DOI: 10.1021/acsami.5b04315
ACS Appl. Mater. Interfaces 2015, 7, 22181−22187

(6) Safavy, A.; Raisch, K. P.; Mantena, S.; Sanford, L. L.; Sham, S. W.; Krishna, N. R.; Bonner, J. A. Design and Development of Water-Soluble Curcumin Conjugates as Potential Anticancer Agents. *J. Med. Chem.* **2007**, *50*, 6284−6288.
(7) Aggarwal, S.; Ndinguri, M. W.; Solipuram, R.; Wakamatsu, N.; Hammer, R. P.; Ingram, D.; Hansel, W. [DLys(6)]-Luteinizing Hormone Releasing Hormone-Curcumin Conjugate Inhibits Pancreatic Cancer Cell Growth in vitro and in vivo. *Int. J. Cancer* **2011**, *129*, 1611−1623.
(8) Ravindran, J.; Prasad, S.; Aggarwal, B. B. Curcumin and Cancer Cells: How Many Ways Can Curry Kill Tumor Cells Selectively? *AAPS J.* **2009**, *11*, 495−510.
(9) Chin, S. F.; Iyer, K. S.; Saunders, M.; St. Pierre, T. G.; Buckley, C.; Paskevicius, M.; Raston, C. L. Encapsulation and Sustained Release of Curcumin Using Superparamagnetic Silica Reservoirs. *Chem. - Eur. J.* **2009**, *15*, 5661−5665.
(10) Harada, T.; Giorgio, L.; Harris, T. J.; Pham, D. T.; Ngo, H. T.; Need, E. F.; Coventry, B. J.; Lincoln, S. F.; Easton, C. J.; Buchanan, G.; Kee, T. W. Diamide Linked Gamma-Cyclodextrin Dimers as Molecular-Scale Delivery Systems for The Medicinal Pigment Curcumin to Prostate Cancer Cells. *Mol. Pharmaceutics* **2013**, *10*, 4481−4490.
(11) Sahu, A.; Kasoju, A.; Bora, U. Fluorescence Study of the Curcumin-Casein Micelle Complexation and Its Application as a Drug Nanocarrier to Cancer Cells. *Biomacromolecules* **2008**, *9*, 2905−2912.
(12) Zhao, J.; Liu, J.; Xu, S.; Zhou, J.; Han, S.; Deng, L.; Zhang, J.; Liu, J.; Meng, A.; Dong, A. Graft Copolymer Nanoparticles with pH and Reduction Dual-Induced Disassemblable Property for Enhanced Intracellular Curcumin Release. *ACS Appl. Mater. Interfaces* **2013**, *5*, 13216−13226.
(13) Misra, R.; Sahoo, S. K. Coformulation of Doxorubicin and Curcumin in Poly(D,L-Lactide-co-Gglycolide) Nanoparticles Suppresses the Development of Multidrug Resistance in K562 Cells. *Mol. Pharmaceutics* **2011**, *8*, 852−866.
(14) Luo, Z.; Tikekar, R. V.; Nitin, N. Click Chemistry Approach for Imaging Intracellular and Intratissue Distribution of Curcumin and its Nanoscale Carrier. *Bioconjugate Chem.* **2014**, *25*, 32−42.
(15) Lazar, A. N.; Mourtas, S.; Youssef, I.; Parizot, C.; Dauphin, A.; Delatour, B.; Antimisiaris, S. G.; Duyckaerts, C. Curcumin-Conjugated Nanoliposomes with High Affinity for Abeta Deposits: Possible Applications to Alzheimer Disease. *Nanomedicine* **2013**, *9*, 712−721.
(16) Dhule, S. S.; Penfornis, P.; He, J.; Harris, M. R.; Terry, T.; John, V.; Pochampally, R. The Combined Effect of Encapsulating Curcumin and C6 Ceramide in Liposomal Nanoparticles against Osteosarcoma. *Mol. Pharmaceutics* **2014**, *11*, 417−427.
(17) Li, B.; Wen, H.; Zhou, W.; Chen, B. Porous Metal−Organic Frameworks for Gas Storage and Separation. *J. Phys. Chem. Lett.* **2014**, *5*, 3468−3479.
(18) Wang, C.; Liu, D.; Lin, W. Metal-Organic Frameworks as A Tunable Platform for Designing Functional Molecular Materials. *J. Am. Chem. Soc.* **2013**, *135*, 13222−31224.
(19) Burtch, N. C.; Jasuja, H.; Walton, K. S. Water Stability and Aadsorption in Metal-Organic Frameworks. *Chem. Rev.* **2014**, *114*, 10575−10612.
(20) Wang, C.; Zhang, T.; Lin, W. Rational Synthesis of Noncentrosymmetric Metal-Organic Frameworks for Second-Order Nonlinear Optics. *Chem. Rev.* **2012**, *112*, 1084−1104.
(21) Furukawa, H.; Muller, U.; Yaghi, O. M. "Heterogeneity within Order" in Metal-Organic Frameworks. *Angew. Chem., Int. Ed.* **2015**, *54*, 3417−3430.
(22) Zhang, Q.; Shreeve, J. M. Metal-Organic Frameworks as High Explosives: A New Concept for Energetic Materials. *Angew. Chem., Int. Ed.* **2014**, *53*, 2540−2542.
(23) Banerjee, R.; Phan, A.; Wang, B.; Knobler, C.; Furukawa, H.; O'Keeffe, M.; Yaghi, O. M. High-Throughput Synthesis of Zeolitic Imidazolate Frameworks and Application to CO_2 Capture. *Science* **2008**, *319*, 939−943.
(24) Falkowski, J. M.; Sawano, T.; Zhang, T.; Tsun, G.; Chen, Y.; Lockard, J. V.; Lin, W. Privileged Phosphine-Based Metal-Organic Frameworks for Broad-Scope Asymmetric Catalysis. *J. Am. Chem. Soc.* **2014**, *136*, 5213−5216.
(25) Hu, A.; Liu, S.; Lin, W. Immobilization of Chiral Catalysts on Magnetite Nanoparticles for Highly Enantioselective Asymmetric Hydrogenation of Aromatic Ketones. *RSC Adv.* **2012**, *2*, 2576−2580.
(26) Manna, K.; Zhang, T.; Lin, W. Postsynthetic Metalation of Bipyridyl-Containing Metal-Organic Frameworks for Highly Efficient Catalytic Organic Transformations. *J. Am. Chem. Soc.* **2014**, *136*, 6566−6569.
(27) Manna, K.; Zhang, T.; Carboni, M.; Abney, C. W.; Lin, W. Salicylaldimine-Based Metal-Organic Framework Enabling Highly Active Olefin Hydrogenation with Iron and Cobalt Catalysts. *J. Am. Chem. Soc.* **2014**, *136*, 13182−13185.
(28) Liu, Y.; Xi, X.; Ye, C.; Gong, T.; Yang, Z.; Cui, Y. Chiral Metal-Organic Frameworks Bearing Free Carboxylic Acids for Organocatalyst Encapsulation. *Angew. Chem., Int. Ed.* **2014**, *53*, 13821−13825.
(29) Zheng, M.; Liu, Y.; Wang, C.; Liu, S.; Lin, W. Cavity-Induced Enantioselectivity Reversal in A Chiral Metal−Organic Framework Brønsted Acid Catalyst. *Chem. Sci.* **2012**, *3*, 2623−2627.
(30) Kozachuk, O.; Luz, I.; Xamena, F. X. L.; Noei, H.; Kauer, M.; Albada, H. B.; Bloch, E. D.; Marler, B.; Wang, Y.; Muhler, M.; Fischer, R. A. Multifunctional, Defect-Engineered Metal−Organic Frameworks with Ruthenium Centers: Sorption and Catalytic Properties. *Angew. Chem., Int. Ed.* **2014**, *53*, 7058−7062.
(31) Li, R.; Hu, J.; Deng, M.; Wang, H.; Wang, X.; Hu, Y.; Jiang, H. L.; Jiang, J.; Zhang, Q.; Xie, Y.; Xiong, Y. Integration of An Inorganic Semiconductor with A Metal-Organic Framework: A Platform for Enhanced Gaseous Photocatalytic Reactions. *Adv. Mater.* **2014**, *26*, 4783−4788.
(32) Zhang, W.; Lu, G.; Cui, C.; Liu, Y.; Li, S.; Yan, W.; Xing, C.; Chi, Y. R.; Yang, Y.; Huo, F. A Family of Metal-Organic Frameworks Exhibiting Size-Selective Catalysis with Encapsulated Noble-Metal Nanoparticles. *Adv. Mater.* **2014**, *26*, 4056−4060.
(33) Wang, S.; Yao, W.; Lin, J.; Ding, Z.; Wang, X. Cobalt Imidazolate Metal-Organic Frameworks Photosplit CO_2 under Mild Reaction Conditions. *Angew. Chem., Int. Ed.* **2014**, *53*, 1034−1038.
(34) Feng, D.; Wang, K.; Su, J.; Liu, T. F.; Park, J.; Wei, Z.; Bosch, M.; Yakovenko, A.; Zou, X.; Zhou, H. C. A Highly Stable Zeotype Mesoporous Zirconium Metal-Organic Framework with Ultralarge Pores. *Angew. Chem., Int. Ed.* **2015**, *54*, 149−154.
(35) Luo, F.; Fan, C. B.; Luo, M. B.; Wu, X. L.; Zhu, Y.; Pu, S. Z.; Xu, W. Y.; Guo, G. C. Photoswitching CO_2 Capture and Release in A Photochromic Diarylethene Metal-Organic Framework. *Angew. Chem., Int. Ed.* **2014**, *53*, 9298−301.
(36) Lim, D. W.; Chyun, S. A.; Suh, M. P. Hydrogen Storage in A Potassium-Ion-Bound Metal-Organic Framework Incorporating Crown Ether Struts as Specific Cation Binding Sites. *Angew. Chem., Int. Ed.* **2014**, *53*, 7819−7822.
(37) DeCoste, J. B.; Weston, M. H.; Fuller, P. E.; Tovar, T. M.; Peterson, G. W.; LeVan, M. D.; Farha, O. K. Metal-Organic Frameworks for Oxygen Storage. *Angew. Chem., Int. Ed.* **2014**, *53*, 14092−14095.
(38) Bezuidenhout, C. X.; Smith, V. J.; Bhatt, P. M.; Esterhuysen, C.; Barbour, L. J. Extreme Carbon Dioxide Sorption Hysteresis in Open-Channel Rigid Metal-Organic Frameworks. *Angew. Chem., Int. Ed.* **2015**, *54*, 2079−2083.
(39) Liu, D.; Gu, J.; Liu, Q.; Tan, Y.; Li, Z.; Zhang, W.; Su, Y.; Li, W.; Cui, A.; Gu, C.; Zhang, D. Metal-Organic Frameworks Reactivate Deceased Diatoms to Be Efficient CO_2 absorbents. *Adv. Mater.* **2014**, *26*, 1229−1234.
(40) Wen, L.; Cheng, P.; Lin, W. Mixed-Motif Interpenetration and Cross-Linking of High-Connectivity Networks. *Chem. Sci.* **2012**, *3*, 2288−2292.
(41) Liu, D.; Wu, H.; Wang, S.; Xie, Z.; Li, J.; Lin, W. A High Connectivity Metal−Organic Framework with Exceptional Hydrogen and Methane Uptake Capacities. *Chem. Sci.* **2012**, *3*, 3032−3037.
(42) Liu, T. F.; Feng, D.; Chen, Y. P.; Zou, L.; Bosch, M.; Yuan, S.; Wei, Z.; Fordham, S.; Wang, K.; Zhou, H. C. Topology-Guided Design and Syntheses of Highly Stable Mesoporous Porphyrinic Zirconium

DOI: 10.1021/acsami.5b04315
ACS Appl. Mater. Interfaces 2015, 7, 22181−22187

Metal-Organic Frameworks with High Surface Area. *J. Am. Chem. Soc.* **2015**, *137*, 413−419.
(43) Xie, Z.; Ma, L.; Kathryn, E.; deKrafft, K. E.; Jin, A.; Lin, W. Porous Phosphorescent Coordination Polymers for Oxygen Sensing. *J. Am. Chem. Soc.* **2010**, *132*, 922−923.
(44) Zheng, M.; Tan, H.; Xie, Z.; Zhang, L.; Jing, X.; Sun, Z. Fast Response and High Sensitivity Europium Metal Organic Framework Fluorescent Probe with Chelating Terpyridine Sites for Fe^{3+}. *ACS Appl. Mater. Interfaces* **2013**, *5*, 1078−1083.
(45) Wanderley, M. M.; Wang, C.; Wu, C. D.; Lin, W. A Chiral Porous Metal-Organic Framework for Highly Sensitive and Enantioselective Fluorescence Sensing of Amino Alcohols. *J. Am. Chem. Soc.* **2012**, *134*, 9050−9053.
(46) Douvali, A.; Tsipis, A. C.; Eliseeva, S. V.; Petoud, S.; Papaefstathiou, G. S.; Malliakas, C. D.; Papadas, I.; Armatas, G. S.; Margiolaki, I.; Kanatzidis, M. G.; Lazarides, T.; Manos, M. J. Turn-on Luminescence Sensing and Real-Time Detection of Traces of Water in Organic Solvents by A Flexible Metal-Organic Framework. *Angew. Chem., Int. Ed.* **2015**, *54*, 1651−1656.
(47) Ye, J.; Zhao, L.; Bogale, R. F.; Gao, Y.; Wang, X.; Qian, X.; Guo, S.; Zhao, J.; Ning, G. Highly Selective Detection of 2,4,6-Trinitrophenol and Cu^{2+} Ions Based on A Fluorescent Cadmium-Pamoate Metal-Organic Framework. *Chem. - Eur. J.* **2015**, *21*, 2029−2037.
(48) Joarder, B.; Desai, A. V.; Samanta, P.; Mukherjee, S.; Ghosh, S. K. Selective and Sensitive Aqueous-Phase Detection of 2,4,6-Trinitrophenol (TNP) by an Amine-Functionalized Metal-Organic Framework. *Chem. - Eur. J.* **2015**, *21*, 965−969.
(49) Cui, J.; Wong, Y. L.; Zeller, M.; Hunter, A. D.; Xu, Z. Pd Uptake and H_2S Sensing by An Amphoteric Metal-Organic Framework with A Soft Core and Rigid Side Arms. *Angew. Chem., Int. Ed.* **2014**, *53*, 14438−14442.
(50) Li, X.; Xu, H.; Kong, F.; Wang, R. A Cationic Metal-Organic Framework Consisting of Nanoscale Cages: Capture, Separation, and Luminescent Probing of $Cr_2O_7^{2-}$ through A Single-Crystal to Single-Crystal Process. *Angew. Chem., Int. Ed.* **2013**, *52*, 13769−13773.
(51) Tan, H.; Liu, B.; Chen, Y. Lanthanide Coordination Polymer Nanoparticles for Sensing of Mercury (II) by Photoinduced Electron Transfer. *ACS Nano* **2012**, *6*, 10505−10511.
(52) Chen, G.; Liu, D.; He, C.; Gannett, T. R.; Lin, W.; Weizmann, Y. Enzymatic Synthesis of Periodic DNA Nanoribbons for Intracellular pH Sensing and Gene Silencing. *J. Am. Chem. Soc.* **2015**, *137*, 3844−3851.
(53) deKrafft, K. E.; Xie, Z.; Cao, G.; Tran, S.; Ma, L.; Zhou, O. Z.; Lin, W. Iodinated Nanoscale Coordination Polymers as Potential Contrast Agents for Computed Tomography. *Angew. Chem., Int. Ed.* **2009**, *48*, 9901−9904.
(54) He, C.; Lu, K.; Lin, W. Nanoscale Metal-Organic Frameworks for Real-Time Intracellular pH Sensing in Live Cells. *J. Am. Chem. Soc.* **2014**, *136*, 12253−12256.
(55) He, C.; Lu, K.; Liu, D.; Lin, W. Nanoscale Metal-Organic Frameworks for The Co-Delivery of Cisplatin and Pooled siRNAs to Enhance Therapeutic Efficacy in Drug-Resistant Ovarian Cancer Cells. *J. Am. Chem. Soc.* **2014**, *136*, 5181−5184.
(56) Huxford, R. C.; Dekrafft, K. E.; Boyle, W. S.; Liu, D.; Lin, W. Lipid-Coated Nanoscale Coordination Polymers for Targeted Delivery of Antifolates to Cancer Cells. *Chem. Sci.* **2012**, *3*, 198−204.
(57) Taylor-Pashow, K. M. L.; Rocca, J. D.; Xie, Z.; Tran, S.; Lin, W. Postsynthetic Modifications of Iron-Carboxylate Nanoscale Metal-Organic Frameworks for Imaging and Drug Delivery. *J. Am. Chem. Soc.* **2009**, *131*, 14261−14263.
(58) Lu, K.; He, C.; Lin, W. Nanoscale Metal-organic Framework for Highly Effective Photodynamic Therapy of Resistant Head and Neck Cancer. *J. Am. Chem. Soc.* **2014**, *136*, 16712−16715.
(59) Rocca, J. D.; Liu, D.; Lin, W. Nanoscale Metal Organic Frameworks for Biomedical Imaging and Drug Delivery. *Acc. Chem. Res.* **2011**, *44*, 957−968.
(60) Liu, Y.; Tang, Z. Nanoscale Biocoordination Polymers: Novel Materials from An Old Topic. *Chem. - Eur. J.* **2012**, *18*, 1030−1037.
(61) Lu, G.; Li, S.; Guo, Z.; Farha, O. K.; Hauser, B. G.; Qi, X.; Wang, Y.; Wang, X.; Han, S.; Liu, X.; DuChene, J. S.; Zhang, H.; Zhang, Q.; Chen, X.; Ma, J.; Loo, S. C.; Wei, W. D.; Yang, Y.; Hupp, J. T.; Huo, F. Imparting Functionality to A Metal-Organic Framework Material by Controlled Nanoparticle Encapsulation. *Nat. Chem.* **2012**, *4*, 310−316.
(62) Venna, S. R.; Jasinski, J. B.; Carreon, M. A. Structural Evolution of Zeolitic Imidazolate Framework-8. *J. Am. Chem. Soc.* **2010**, *132*, 18030−18033.
(63) Tan, J. C.; Bennett, T. D.; Cheetham, A. K. Chemical Structure, Network Topology, and Porosity Effects on the Mechanical Properties of Zeolitic Imidazolate Frameworks. *Proc. Natl. Acad. Sci. U. S. A.* **2010**, *107*, 9938−9943.
(64) Ren, H.; Zhang, L.; An, J.; Wang, T.; Li, L.; Si, X.; He, L.; Wu, X.; Wang, C.; Su, Z. Polyacrylic Acid@Zeolitic Imidazolate Framework-8 Nanoparticles with Ultrahigh Drug Loading Capability for pH-Sensitive Drug Release. *Chem. Commun.* **2014**, *50*, 1000−1002.
(65) Vasconcelos, I. B.; da Silva, T. G. d.; Militão, G. C. G.; Soares, T. A.; Rodrigues, N. M.; Rodrigues, M. O.; da Costa, N. B., Jr.; Freire, R. O.; Junior, S. A. Cytotoxicity and Slow Release of The Anti-Cancer Drug Doxorubicin from ZIF-8. *RSC Adv.* **2012**, *2*, 9437−9442.
(66) Zhuang, J.; Kuo, C.-H.; Chou, L.-Y.; Liu, D.-Y.; Weerapana, E.; Tsung, C.-K. Optimized Metal Organic-Framework Nanospheres for Drug Delivery: Evaluation of Small-Molecule Encapsulation. *ACS Nano* **2014**, *8*, 2812−2819.
(67) Park, K. S.; Ni, Z.; Cote, A. P.; Choi, J. Y.; Huang, R.; Uribe-Romo, F. J.; Chae, H. K.; O'Keeffe, M.; Yaghi, O. M. Exceptional Chemical and Thermal Stability of Zeolitic Imidazolate Frameworks. *Proc. Natl. Acad. Sci. U. S. A.* **2006**, *103*, 10186−10191.
(68) Kobayashi, H.; Watanabe, R.; Choyke, P. L. Improving Conventional Enhanced Permeability and Retention (EPR) Effects: What is The Appropriate Target? *Theranostics* **2014**, *4*, 81−89.
(69) Upreti, M.; Jyoti, A.; Sethi, P. Tumor Microenvironment and Nanotherapeutics. *Transl. Cancer. Res.* **2013**, *2*, 309−319.

DOI: 10.1021/acsami.5b04315
ACS Appl. Mater. Interfaces 2015, 7, 22181−22187